2023 62nd IEEE Conference on Decision and Control (CDC)
December 13-15, 2023. Marina Bay Sands, Singapore

# A negative imaginary approach for distributed secondary frequency consensus control of networked AC microgrids

Arijit Ganguly, Adino W. Ayele, Parijat Bhowmick and Alexander Lanzon, *Senior Member, IEEE*

***Abstract*— This paper proposes a new Secondary Frequency Consensus (SFC) control scheme for inverter-based AC microgrids relying on Negative Imaginary (NI) systems theory. A microgrid consists of many Distributed Generating (DG) units whose dynamics can be modelled by a set of nonlinear differential-algebraic equations. Each DG can be feedback-linearised into a single integrator system, which resembles the simplified frequency dynamics of a microgrid. A network of many such feedback-linearised DG units gives rise to a homogeneous NI multi-agent system (MAS). Interestingly, a single-integrator MAS, owing to be NI, can be conveniently stabilised by a distributed Strictly NI (SNI) controller depending only on the definiteness of the DC gain matrix of the controller. It also successfully achieves the consensus, resulting in frequency synchronisation among all DG units and the main grid. An in-depth Matlab simulation case study was carried out to test the usefulness and performance of the proposed scheme.**

## I. Introduction

Microgrid, a small-scale power network, is formed by solar/battery-powered Distributed Generation (DG) units consisting of power-electronic converters that convert the DC source power into AC power to supply the connected loads. The DGUs must maintain a strong synchronisation to counteract any deviation or fluctuations in the line voltage or frequency and ensure a prescribed power quality [1], [2]. Microgrids/smart grids execute primary and secondary voltage and frequency control policies to achieve these objectives. Primary control preserves the overall grid stability during the line voltage or frequency fluctuations, while secondary control nullifies any deviations in the voltage or frequency from their reference values. Therefore, the secondary voltage and frequency control of microgrids/smart grids drew serious attention from academia and industry. With the advent of Multi-agent Systems (MAS) theory and distributed cooperative control techniques, the secondary control problem has found new and effective solutions. Eventually, it has become a promising research topic in the MAS domain.

This work was supported by the Engineering and Physical Sciences Research Council (EPSRC) [grant number EP/R008876/1] and the Science and Engineering Research Board (SERB), DST, India [grant number SRG/2022/000892]. All research data supporting this publication are directly available within this publication. For the purpose of open access, the authors have applied a Creative Commons Attribution (CC BY) licence to any Author Accepted Manuscript version arising.

A. Ganguly is with the Dept. of EE, University of Engineering and Management Kolkata, West Bengal, India; P. Bhowmick and A. W. Ayele are with the Dept. of EEE, IIT Guwahati, Assam–781039, India; A. Lanzon is with the Dept. of EEE, School of Engineering, University of Manchester, Manchester M13 9PL, UK. Emails: arijit.ganguly@uem.edu.in, a.adino@iitg.ac.in, parijat.bhowmick@iitg.ac.in, Alexander.Lanzon@manchester.ac.uk.

Negative Imaginary (NI) systems theory was conceived in 2007-08, inspired by the positive position feedback control of lightly damped mechanical systems [3]. Besides its most vital application in vibration control, NI theory has established its worth in solving a variety of engineering problems, such as control of nano-positioning systems [4], control of various networked multi-agent systems [6]–[8], train platooning [5], etc. The primary advantage of the NI toolkit is its simple closed-loop stability condition [$\lambda_{\max}\big(N(0)M(0)\big) < 1$] that depends on the loop gain only at $\omega = 0$ [3]. Moreover, it offers a stand-alone robust stability analysis and controller synthesis framework [3], [10]. The latest theoretical advancements of the NI theory include dissipative characterisation of Input and/or Output NI systems [11]–[15].

This paper has utilised the NI theory to develop a new Secondary Frequency Consensus (SFC) control scheme for an AC microgrid comprising networked DG units. Unlike the commonly-used Lyapunov theory-based cooperative control schemes, the NI theory-based SFC scheme relies on the NI-SNI stability result and exploits the Characteristic Loci (also called Eigenvalue Loci) technique [18] to prove the consensus. Hence, the latter does not need to search for an appropriate Lyapunov function, which significantly reduces the theoretical complexity and renders an easy implementation. The proposed scheme uses an LTI dynamic output feedback SNI controller, and therefore, it does not suffer from any discontinuous control action (which is often the cause of the chattering phenomenon), unlike many well-known cooperative control protocols. In the end, we compared the efficacy of the proposed scheme with some of the extensively-used SFC control protocols [20]–[23].

## II. Preliminaries and problem formation

### A. NI and SNI nomenclature

This subsection includes the frequency-domain definitions of NI and SNI systems.

*Definition 1:* (**NI System**) [9], [10] A system $\Sigma(s) \in \mathscr{R}^{m\times m}$ with no poles in $\{s \in \mathbb{C} : \Re[s] > 0\}$ is NI if $j[\Sigma(j\omega) - \Sigma(j\omega)^*] \geq 0 \ \forall\omega \in (0,\infty)$ except those $\omega_0 \in \omega$ where $s = j\omega_0$ is a pole of $\Sigma(s)$. If $\omega_0 \in (0,\infty)$, the multiplicity of the pole $(s^2 + \omega_0^2)$ cannot be more than one and the residue matrix $\Delta|_{s=j\omega_0} \triangleq \lim_{s\to j\omega_0}(s - j\omega_0)j\Sigma(s) = \Delta|^*_{s=j\omega_0} \geq 0$. If $s = 0$ is a pole of $\Sigma(s)$, then $\lim_{s\to 0} s^k\Sigma(s) = 0 \ \forall k \geq 3$ and the residue matrix $\Delta|_{s=0} \triangleq \lim_{s\to 0} s^2\Sigma(s)\Delta|^*_{s=0} \geq 0$.

*Definition 2:* (**SNI System**) [3], [9] A system $\Sigma(s) \in \mathscr{RH}_\infty^{m\times m}$ is SNI if $j[\Sigma(j\omega) - \Sigma(j\omega)^*] > 0 \ \forall\omega \in (0,\infty)$.

2023 62nd IEEE Conference on Decision and Control (CDC) | 979-8-3503-0124-3/23/$31.00 ©2023 IEEE | DOI: 10.1109/CDC49753.2023.10383885

### B. Properties of multi-agent NI systems

We will now mention a few crucial properties to be satisfied by a multi-agent NI system.

*Property 1:* The interaction topology among the $N$ homogeneous NI agents is described by an undirected and connected graph $\mathscr{G}$. There always exists a root node (also called the *leader*) that provides reference command to all the remaining nodes of $\mathscr{G}$ directly or indirectly.

Owing to Property 1, the graph Laplacian matrix enjoys the property $(\mathscr{L}+\mathbb{G})>0$ in the homogeneous case where $\mathbb{G}=\text{diag}\{g_1,g_2,\cdots,g_N\}>0$ is the pinning-gain matrix. The element $g_i$ for $i\in\{1,2,\ldots,N\}$ in $\mathbb{G}$ gives the weight of the interaction edge connecting a root node (labelled as '0') and the $i^{\text{th}}$ agent. The following lemma proves that a homogeneous multi-agent NI (resp. SNI) system satisfying Property 1 retains the NI (resp. SNI) property. The concept was first proved in [6] and later used in many other papers.

*Lemma 1:* [6]–[8], [16], [17] Consider a homogeneous multi-agent NI (resp. SNI) system with Property 1. Then, $\bar{M}(s)=(\mathscr{L}+\mathbb{G})\otimes M(s)$ is NI (resp. SNI) $\Leftrightarrow$ $M(s)$ is NI (resp. SNI).

Lemma 2 shows that a network of all homogeneous stable NI (including SNI) systems retains the same sign definiteness of its DC-gain matrix when the corresponding interaction topology satisfies Property 1.

*Lemma 2:* [6], [16], [17] Consider a network of $N$ identical stable NI agents $M(s)\in\mathscr{RH}_\infty^{m\times m}$ satisfying Property 1. Denote $\bar{M}(s)=(\mathscr{L}+\mathbb{G})\otimes M(s)$. Then, $\bar{M}(0)>0$ (resp. $<0$) if and only if $M(0)>0$ (resp. $<0$).

### C. Characteristic loci theory

The concept of *characteristic loci* and its application in determining closed-loop asymptotic stability of LTI MIMO systems were introduced during 1969–1973 by MacFarlane and Belletrutti [18], [19]. This concept is analogous to a *multi-loop* Nyquist criterion that offers a pretty convenient graphical stability analysis tool for MIMO systems. The characteristic loci $\lambda_i(s)$, where $i\in\{1,2,\ldots,m\}$, of any square LTI system $\Sigma(s)\in\mathscr{R}^{m\times m}$ is a conformal mapping of the complex function $\det[\Sigma(s)]$ into another complex plane when $s$ follows the standard $s$-plane $D$-contour in a CW direction (see Fig. 2a).

*Theorem 1:* [18], [19] A necessary and sufficient criterion for a closed-loop interconnection of two LTI systems $\Sigma(s)$ and $\Sigma_c(s)$, connected via a negative feedback, to maintain asymptotic stability is that the total number of the CCW encirclements about the $(-1+j0)$ point by the characteristic loci $\lambda_i(j\omega)$ of $L(s)\triangleq\Sigma(s)\Sigma_c(s)$ $\forall i\in\{1,2,\ldots,n\}$ should be equal to the number of RHP poles of $L(s)$. When $L(s)\in\mathscr{RH}_\infty$, none of the characteristic loci $\lambda_i(j\omega)$ should encircle the $(-1+j0)$ point.

### D. Problem formation

This paper seeks to design a distributed secondary frequency control consensus scheme for inverter-based AC microgrids applying the Negative Imaginary control technique. It has been shown via simulation case studies that the proposed scheme offers a certain degree of robustness to high-frequency noises and sudden loss of DGs.

## III. Modelling of an Inverter-Based Microgrid

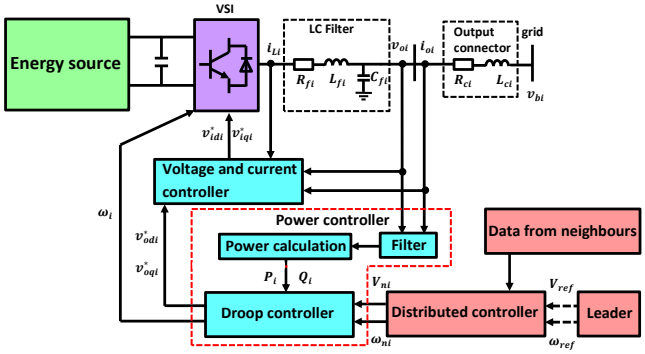


Fig. 1. Schematic diagram of an inverter-based DG unit, including PI-type primary droop controller and secondary frequency controller.

The schematic block diagram of a DG unit of a microgrid is shown in Fig. 1 and the concept has been taken from [20], [21]. The following notations are used in this figure and in the mathematical model (1) – $\omega_i$ denotes the angular frequency of the $i^{\text{th}}$ DG. $\phi_i$ is the angle of the $i^{\text{th}}$ DG reference frame w.r.t. the common reference frame. $P_i$ and $Q_i$ are the measured active and reactive power at the DG terminal. $\omega_{n_i}$ and $\nu_{n_i}$ are the primary control references. $V^*_{odi}$, $V^*_{oqi}$ form the references of the voltage and current controllers respectively. $\psi_{d_i}$, $\psi_{q_i}$, $\lambda_{d_i}$ and $\lambda_{q_i}$ are defined as the auxiliary state variables associated with the voltage and current PI controllers. $R_{fi}$, $C_{fi}$, $L_{fi}$ denotes the parameters of the output filter and $R_{ci}$, $L_{ci}$ forms the output connector. $V_{bi}$ is the bus voltage. $V^*_{idi}$ and $V^*_{iqi}$ are the output of current controller of the $i^{\text{th}}$ DG along d-q axis. $i_{Li}$ is the line current of the $i^{\text{th}}$ DG unit and $v_{oi}$ and $i_{oi}$ are the output voltage and current of the $i^{\text{th}}$ DG respectively. As derived in [21] and [20], each DG unit is governed by a set of nonlinear differential-algebraic equations given below:

$$\Sigma_{DG}:\begin{cases}\dot{\boldsymbol{x}}_i=\boldsymbol{f}_i(\boldsymbol{x}_i)+\boldsymbol{g}_i(\boldsymbol{x}_i)u_i+\boldsymbol{d}_i(\boldsymbol{x}_i)\mathbb{W}_i\\ y_i=\boldsymbol{h}_i(\boldsymbol{x}_i)\end{cases}\tag{1}$$

for all $i\in\{1,2,\ldots,N\}$ where the state vector is defined as

$$\boldsymbol{x}_i=\big[\phi_i\ P_i\ Q_i\ \psi_{d_i}\ \psi_{q_i}\ \lambda_{d_i}\ \lambda_{q_i}\ I_{Ldi}\ I_{Lqi}\ V_{odi}\ V_{oqi}\ I_{odi}\ I_{oqi}\big]^\top$$

and $\mathbb{W}_i$ stands for the exogenous disturbance. The model given in (1) is nonlinear. An appropriate input-output feedback linearising control law [21] is therefore used to find a linearised model of the frequency dynamics of each DG. The expression below reveals the relationship between the frequency ($\omega_i$) and the auxiliary control input ($v_{f_i}$)

$$\dot{\omega}_i=v_{f_i}\qquad\forall i\in\{1,2,\ldots,N\}.\tag{2}$$

## IV. An NI-based distributed secondary frequency consensus control scheme

This section presents the fundamental results of this paper. A new consensus control methodology has been proposed relying on the NI theory and the characteristic loci technique and it has been used to achieve secondary frequency control of inverter-based AC microgrid systems comprised of many DG units. These DG units are not only physically connected but also connected in a cyber layer via a network. Each DG unit is considered as an agent (or a node) in the multi-agent systems framework. This paper assumes a bidirectional connection among the DG units, for which the graph Laplacian matrix $\mathscr{L}$ enjoys the property $\mathscr{L} = \mathscr{L}^\top \geq 0$.

For the DG units, the goal of reaching the same desired frequency $r = \omega_{\text{ref}}$ is nothing but a leader-following consensus-seeking problem. The interaction edge between a reference node and the $i^{\text{th}}$ agent has a positive weight $g_i > 0$. The matrix containing all such weights is called the pinning-gain matrix $\mathbb{G} = \text{diag}\{g_1, g_2, \cdots, g_N\} > 0$. We assume that the communication topology among the agents is strongly connected and at least one agent (i.e. a DG unit) should be directly connected to the reference node. Under this assumption, the graph $\mathscr{G}$ satisfies the property $\mathscr{L} + \mathbb{G} > 0$. In case of a direction communication topology, we require the existence of a spanning tree such that all the agents in a network are directly or indirectly connected to the reference node. Although in this paper, we have considered the bidirectional graph, but the work can be readily extended to the case of a directed topology.

Fig. 3a shows the two-loop configuration for implementing the proposed secondary frequency consensus (SFC) control scheme on a networked microgrids where as Fig. 3c shows the NI theory-based SFC control scheme. Theorem 2 develops the theoretical basis and proof of the proposed scheme, which is the primary contribution of this paper.

*Theorem 2:* Consider a homogeneous network of $N$ DG units in an inverter-based AC microgrid whose feedback-linearised frequency dynamics is governed by the equation $\dot{\omega}_i = v_{f_i}$ for $i \in \{1, 2, \ldots, N\}$. Let the reference be $\mathbf{r} = \mathbf{1}\omega_{\text{ref}}$. Choose an SNI controller $\Sigma_c(s)$ with $\Sigma_c(0) > 0$ for the scheme shown in Fig. 3c. Then, there always exists a finite $\beta \in (0, \beta^*]$ such that all DGs in the microgrid achieve secondary frequency consensus by the following distributed SNI control law

$$u_i = \beta \Sigma_c(s) \sum_{j=1}^{N} a_{ij}(y_i - y_j) + g_i(y_i - r) \tag{3}$$

for all $i \in \{1, 2, \ldots, N\}$

**Proof.** We have divided the proof into two major parts – Part I derives the asymptotic stability of the consensus control scheme and Part II shows that the consensus error asymptotically decays to zero.

**Part 1: Asymptotic stability of the scheme**

The scheme shown in Fig. 3c has been developed to achieve a leader-following consensus, which has the loop transfer function $T_L = (\mathscr{L} + \mathbb{G}) \otimes \frac{1}{s}\Sigma_c(s)$. The symbol $\bar{\lambda}_i(s)$ represents the characteristic loci of $T_L$ where $i \in \{1, 2, \ldots, N\}$. To proceed with the proof, three sets $\Psi_0$, $\Psi_{\pm\Im}$ and $\Psi_\infty$ of the Laplace variable $s$ are defined corresponding to three specific regions marked in Fig. 2b along the standard $s$-plane $D$-contour. To prove the asymptotic stability of the proposed consensus control scheme, we will exploit the characteristic loci theorem (Theorem 1). This proof consists of the following three cases.

**Case 1:** For the subset $s \in \Psi_0$

We can approximately express the characteristic loci $\bar{\lambda}_i(s)$

$$\bar{\lambda}_i(s)|_{s\in\Psi_0} \simeq \lambda_i\left[(\mathscr{L} + \mathbb{G}) \otimes \Sigma_c(0)\right] \frac{1}{\varepsilon} e^{-j\theta} \tag{4}$$

where $\lambda_i$ simply denotes the $i^{\text{th}}$ eigenvalue of a real matrix. Let $\lambda_i\left[(\mathscr{L} + \mathbb{G}) \otimes \Sigma_c(0)\right] = c_i e^{j\phi_i}$ where $\phi_i = 0\ \forall i$ since $\Sigma_c(0) > 0$ and $(\mathscr{L} + \mathbb{G}) > 0$. Then, (4) takes the form $\bar{\lambda}_i(s)|_{s\in\Psi_0} \simeq \frac{c_i}{\varepsilon} e^{j(\phi_i - \theta)}$. Therefore, $\bar{\lambda}_i(j0_+) \simeq \frac{c_i}{\varepsilon} e^{-j\frac{\pi}{2}} \to +\infty\angle -\frac{\pi}{2}$ when $\theta = \frac{\pi}{2}$ and considering $\varepsilon \to 0_+$. Similarly, $\bar{\lambda}_i(j0_-) \to +\infty\angle +\frac{\pi}{2}$ when $\theta = -\frac{\pi}{2}$ as the characteristic loci are symmetric about the real axis. This implies $-\frac{\pi}{2} \leq \angle\bar{\lambda}_i(j\omega) \leq +\frac{\pi}{2}\ \forall i$ when $s \in \Omega_0$. Each locus $\bar{\lambda}_i(j\omega)$ connects the $\bar{\lambda}_i(j0_-)$ and $\bar{\lambda}_i(j0_+)$ points (computed at $\omega = 0_+$ and $\omega = 0_-$) in a CW direction through a semicircular arc having radius $\frac{1}{\varepsilon} \to \infty$ as depicted in Fig. 2b. The above analysis guarantees that none of characteristic loci $\bar{\lambda}_i(j\omega)$ crosses the negative real axis at infinity.

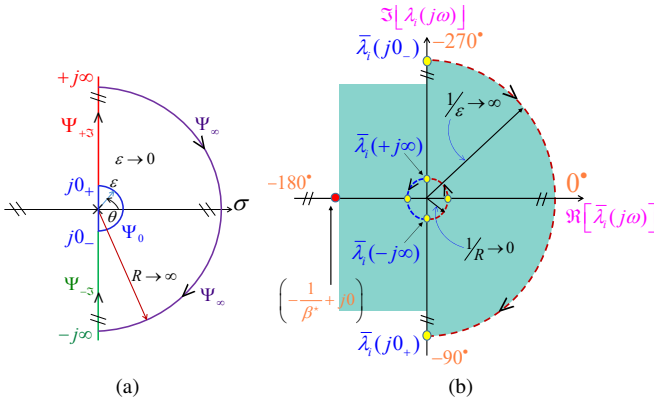


Fig. 2. (a) The standard $s$-plane Nyquist $\mathscr{D}$-contour; and (b) All the characteristic loci $\bar{\lambda}_i(s)$ of $(\mathscr{L} + \mathbb{G}) \otimes \frac{1}{s}\Sigma_c(s)$ lie inside the Sea-Green-coloured region when $\Sigma_c(s)$ is SNI with $\Sigma_c(0) > 0$.

**Case 2:** For the subset $s \in \Psi_{\pm\Im}$

We assume again $\lambda_i\left[(\mathscr{L} + \mathbb{G}) \otimes \Sigma_c(j\omega)\right] = c_i e^{j\phi_i}$ for every $\omega \in (0, \infty)$. Since $\Sigma_c(s)$ is SNI, $\phi_i(\omega) \in (-\pi, 0)\ \forall\omega \in (0, \infty)$ and hence, for all $i$, $\angle\bar{\lambda}_i(j\omega) = (\phi_i - \frac{\pi}{2}) \in \left(-\frac{3\pi}{2}, -\frac{\pi}{2}\right)\ \forall\omega \in (0, \infty)$. Following the same logic, we can assert $\angle\bar{\lambda}_i(j\omega) \in \left(-\frac{3\pi}{2}, -\frac{\pi}{2}\right)$ when $\omega \in (-\infty, 0)$. Ultimately, we can conclude that all $\bar{\lambda}_i(j\omega)$ stay inside the rectangular Sea-Green-coloured zone in the open left-half plane (marked in Fig. 2b) when $s \in \Psi_{\pm\Im}$. We emphasize that none of the $\bar{\lambda}_i(j\omega)$ intersects the negative real axis at infinity.

**Case 3:** For the subset $s \in \Psi_\infty$

Similar to Case I, for this subset also, we can write

$$\bar{\lambda}_i(s)|_{s\in\Psi_\infty} \simeq \lambda_i\left[(\mathscr{L}+\mathbb{G})\otimes\Sigma_c(\infty)\right]\frac{e^{-j\theta}}{R} = \frac{c_i}{R}e^{j(\phi_i-\theta)}$$

upon letting $\lambda_i\left[(\mathscr{L}+\mathbb{G})\otimes\Sigma_c(\infty)\right] = c_i e^{j\phi_i}$ where $\lambda_i$ denotes the eigenvalues. Note that $\phi_i$ can be 0, $-\frac{\pi}{2}$ or $-\pi$ depending on the nature of $\Sigma_c(\infty)$. Note that $\Sigma_c(\infty) = \Sigma_c(\infty)^\top$ since $\Sigma_c(s)$ is an SNI transfer function. Therefore, $\bar{\lambda}_i(+j\infty) \simeq \frac{c_i}{R}e^{j(\phi_i-\frac{\pi}{2})} \to 0\angle -0,\ 0\angle -\frac{\pi}{2}$ or $0\angle -\frac{3\pi}{2}$ as $R\to\infty$. Similarly, $\bar{\lambda}_i(-j\infty)$ also approaches to one of these three possibilities $0\angle -0,\ 0\angle -\frac{\pi}{2}$ or $0\angle -\frac{3\pi}{2}$ when $\theta = -\frac{\pi}{2}$. On the basis of these angle information, we can ascertain that each locus $\bar{\lambda}_i(j\omega)$ joins the $\bar{\lambda}_i(+j\infty)$ and $\bar{\lambda}_i(-j\infty)$ points (computed at $\omega=+\infty$ and $\omega=-\infty$) in the CCW direction via a semicircular arc of radius $\frac{1}{R}\to 0$ as illustrated in Fig. 2b. The above three cases can be combined together to guarantee that all the characteristic loci $\bar{\lambda}_i(s)$ of $T_L(s)$ remain inside the Sea-Green-coloured area marked in Fig. 2b. This is equivalent to saying that there always a finite $\beta^\star > 0$ such that the critical point $(-\frac{1}{\beta}+j0)$ is not encircled by any characteristic locus $\bar{\lambda}_i(s)$ for any $\beta\in(0,\beta^\star]$. This proves asymptotic stability of the consensus error dynamics.

**Part 2: Consensus error decays to zero**

We will now establish the asymptotic convergence of the consensus error $\boldsymbol{\xi} = \begin{bmatrix}\xi_1 & \xi_2 & \cdots & \xi_N\end{bmatrix}^\top$. The error dynamics can be obtained from the block diagram in Fig. 1 as $\boldsymbol{\Xi}(s) = \left[I + \left((\mathscr{L}+\mathbb{G})\otimes\frac{\beta}{s}\Sigma_c(s)\right)\right]^{-1}$. The expression of the time-domain steady-state error can be derived as

$$\begin{aligned}
\boldsymbol{\xi}_{ss} &= \lim_{t\to\infty}\boldsymbol{\xi}(t) = \lim_{s\to 0} s\,\boldsymbol{\Xi}(s)\\
&= \lim_{s\to 0} s\left[I + \left((\mathscr{L}+\mathbb{G})\otimes\frac{\beta}{s}\Sigma_c(s)\right)\right]^{-1}\hat{\mathbf{R}}(s)\\
&= \lim_{s\to 0} s\left[sI + \left((\mathscr{L}+\mathbb{G})\otimes\beta\Sigma_c(s)\right)\right]^{-1}(s\mathbf{R}(s))\\
&= \left[(\mathscr{L}+\mathbb{G})\otimes\beta\Sigma_c(0)\right]^{-1}\left(\lim_{s\to 0} sI\right)\left(\lim_{s\to 0} s\mathbf{R}(s)\right)\\
&= [0\ 0\ \cdots\ 0]^\top
\end{aligned}$$

since $\Sigma_c(0) > 0$, $(\mathscr{L}+\mathbb{G}) > 0$ and $\mathbf{r}(t)$ and $\mathbf{h}(t)$ all are bounded signals for all $t\geq 0$. This hence implies $\lim_{t\to\infty}\xi_i = 0 \Rightarrow \lim_{t\to\infty} y_i(t) = r = \omega_{\text{ref}}$. This completes the proof. ■

## V. MATLAB SIMULATION CASE STUDY AND PERFORMANCE COMPARISON

The microgrid we consider in this case study comprises of four DG units, which communicate among themselves through a network (shown in Fig. 3b) characterised by the Adjacency matrix $\mathscr{A} = [a_{ij}]$ and Laplacian matrix $\mathscr{L} = [l_{ij}]$ where $i,j\in\{1,2,\ldots,N\}$. The reference frequency has been set to $\omega_{\text{ref}} = 1$ pu where 1 pu = 50 Hz. In this case study, we will analyse three different operating conditions: when the microgrid runs in a healthy condition, in a noisy environment and when a DG unit is suddenly disconnected from the network.

**Case 1: Performance under nominal operating condition**

Firstly, we consider that the microgrid is operating under a healthy operating condition, that means the DGs are well-connected and there is no external disturbances or noises. An SNI controller $\Sigma_c(s) = \beta\left(\frac{s+15}{s+14}\right)$ with a coupling gain $\beta = 1600$ is chosen by following Theorem 2 that strictly ensures frequency consensus among the DGs of the microgrid network. The frequency consensus achieved by the control law (3) and the corresponding consensus error are plotted in Fig. 4a and Fig. 4b, which clearly depict that the frequencies $\omega_i$ of the connected DGs perfectly track the reference $\omega_{\text{ref}}$ and meet some desired transient specifications in msec range. Fig. 4c explains that all four DGs are sharing (or delivering) the real/active power in the prescribed ratio of $4:3:2:1$, which must be the inverse of the ratio of the selected droop coefficients $1:1/2:1/3:1/4$.

**Case 2: Performance in a noisy environment**

This subsection tests the performance of the proposed NI-based SFC control scheme in a noisy environment. A noise signal of frequency 300 Hz is applied to the output of DG 1 from $t = 0.002$ sec to $t = 0.004$ sec and a high-frequency noise signal of frequency 2 kHz is also applied to the same DG from $t = 0.011$ sec to $t = 0.033$ sec. Fig. 5a shows the frequency output ($\omega_i$) profiles of all four DGs in the noisy environment and reveals that despite the oscillations (due to the effect of noise) in the $\omega_1$ response, $\omega_2$, $\omega_3$ and $\omega_4$ have successfully achieved the consensus. Fig. 5b shows how fast the consensus error decays to zero. Then, Fig. 5c reports that the real-power-sharing has been maintained at the prescribed ratio $4:3:2:1$ even in the noisy environment.

**Case 3: Effect of a loss of one DG**

In this case also, the microgrid operates with the same network (in Fig. 3b) as considered in the previous two cases. To asses the fault tolerance property of the proposed NI-based SFC control scheme, the microgrid has been allowed to operate with all four DGs up to 0.02 sec in the starting. At $t = 0.02$ sec, DG 4 loses its connection from the network. At $t = 0.03$ sec, reconfiguration of DG 4 again takes place with the considered communication network. After $t = 0.02$ sec, the frequencies of all four DGs reach consensus and remain fixed at $\omega_{\text{ref}}$ again despite a sudden disconnection of one DG unit (i.e. DG 4) from the network for a period of 0.01 sec. The frequencies ($\omega_i$) and active power outputs ($P_i$) of the DGs are shown in Fig. 6 and Fig. 7 respectively.

*Comparison with a renowned existing SFC protocol*

We will now examine the performance of the proposed NI-based SFC scheme against a renowned Lyapunov-based SFC control scheme adopted from [20]–[22]. In this paper, the referred SFC law is named as the *Conventional Cooperative Control* (CCC) protocol and is mentioned below.

$$v_{f_i} = cK_f\,\xi_{f_i} \qquad \forall i\in\{1,2,\ldots,N\} \tag{5}$$

A powerful variant of the above CCC protocol, given in (6), with a pair of adaptive coupling gains ($c_{ad}$ and $\rho_{f_i}$) was exploited in [23] where the weight matrices $Q_f > 0$ and $R_f > 0$ are chosen by the designed, $c_{ad}$ is an adaptive gain

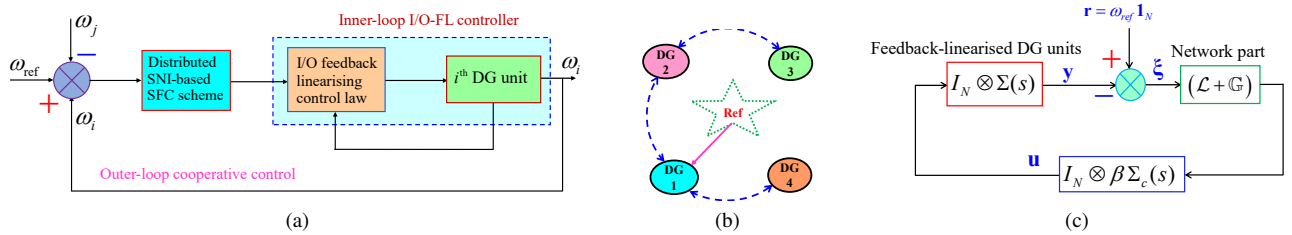


(a) (b) (c)

Fig. 3. (a) A two-loop configuration for implementing the proposed SFC control scheme on a networked microgrid; (b) The interaction topology among the DG units chosen for the case study; and (c) An NI-based SFC control scheme for islanded microgrids.

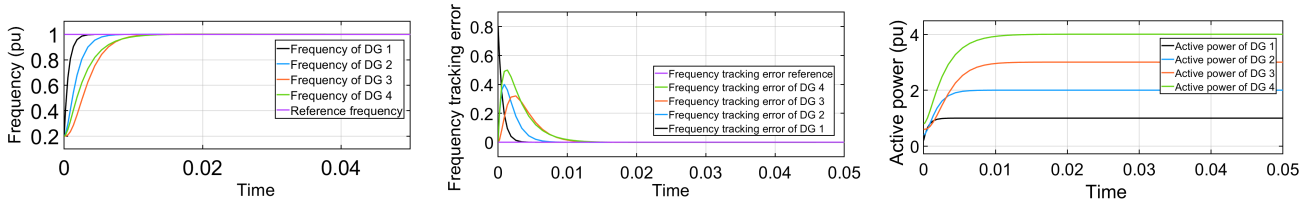


(a) (b) (c)

Fig. 4. (a) Frequency profile ($\omega_1, \omega_2, \omega_3$ and $\omega_4$) of the DGs under the nominal operating condition; (b) Time evolvement of the frequency consensus errors of all four DGs in the nominal operating condition; and (c) Real-power-sharing among the DGs at the desired ratio in the nominal operating condition.

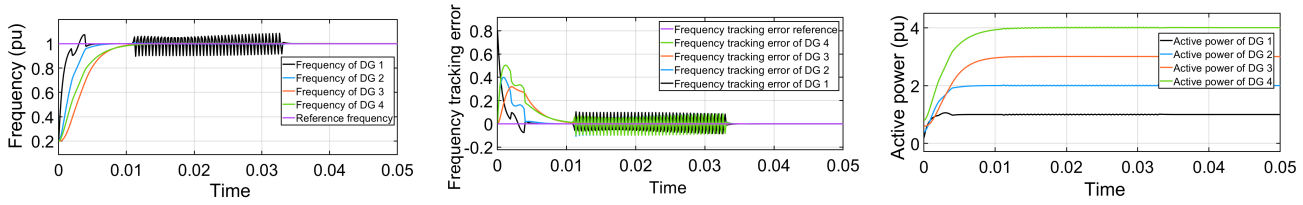


(a) (b) (c)

Fig. 5. (a) Frequency profile of the DGs in a noisy environment; (b) Time evolvement of the frequency consensus errors of all four DGs corresponding to Fig. 5a; and (c) Real-power-sharing among the DGs in the presence of noise.

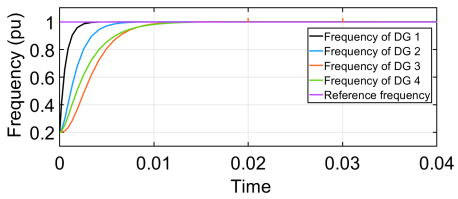


Fig. 6. Frequency profile of the DGs simulated considering a sudden loss of one agent (DG 4).

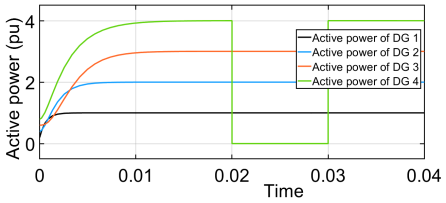


Fig. 7. Real-power-sharing among the DGs considering a sudden loss of one agent (DG 4).

parameter, $K_f$ is the state feedback gain and $\xi_{f_i}$ represents the frequency consensus errors of the DG units.

$$\begin{cases} v_{f_i} = (c_{ad} + \rho_{f_i}) K_f \, \xi_{f_i} \\ \dot{c}_{ad} = Q_f \, \xi_{f_i}^2 \\ K_f = -\sqrt{Q_f / R_f} \text{ and } \rho_{f_i} = \sqrt{Q_f R_f}\, \xi_{f_i}^2 \end{cases} \tag{6}$$

To test the performance of the CCC scheme, we chose $Q_f = 62$ and $R_f = 0.1$, found $K_f = 24.89$ via LQR principle and obtained $\rho_f = 2.49$ by solving the $\dot{c}_{ad}$ dynamics. The frequency consensus achieved by this control law is portrayed in Fig. 8. A comparative study (on the basis of the transient specifications) between the consensus performance

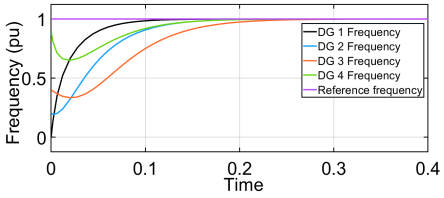


Fig. 8. Frequency consensus of the DGs achieved by the conventional cooperative control (CCC) law given in (5).

achieved by the CCC and NI-based SFC control schemes is given in Table I.

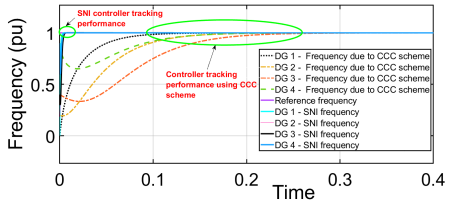


Fig. 9. Reference Comparison-CCC-NI-based-SFC.

TABLE I. Microgrid performance comparison achieved by the conventional cooperative control (CCC) scheme and the proposed SFC control scheme.

| Sl. no. | Criteria | CCC scheme | Proposed scheme | Remarks |
|---|---|---|---|---|
| 1. | Settling time | 0.22s | 0.004s | Improved |
| 2. | Rise time | 0.11s | 0.003s | Improved |
| 3. | % Overshoot | 0 | 0 | Same |
| 4. | Steady-state | 1 | 1 | Same |
| 5. | % Undershoot | 0 | 0 | Same |
| 6. | Peak time | 0.4s | 0.01s | Improved |

Upon comparing Fig. 8 and Fig. 4a, it is pretty clear that the consensus-reaching performance (w.r.t. the transient specifications) in the case of the proposed NI-based SFC scheme (Fig. 4a) is significantly improved than that of the referred CCC scheme. The comparison can be readily observed from Fig. 9 and it has been quantified in Table I.

## VI. Conclusion

This paper has developed a new methodology for a secondary frequency consensus control of inverter-based AC microgrids utilising the NI theory. The primary motivation is that the feedback-linearised frequency dynamics of a DG unit gives a single integrator model, which inherently satisfies the NI property with a pole at the origin. Hence, a microgrid comprising many DG units exhibits multi-agent NI property. A distributed SNI controller can be conveniently designed to stabilise such a network and achieve frequency synchronisation among all the DG units. As the NI framework does not rely on the Lyapunov approach for proving the frequency consensus of the DG units (i.e. the agents), it significantly reduces the theoretical complexity and enables easy implementation. It also facilitates plug-and-play operation and robustness to high-frequency noises. An exhaustive simulation case study was carried out to demonstrate the usefulness of the proposed scheme.

## References


[1] Z. Yang, Y. Li, and J. Xiang, "Coordination control strategy for power management of active distribution networks," *IEEE Transactions on Smart Grid*, vol. 10, no. 5, pp. 5524–5535, 2019.

[2] R. C. Green, L. Wang, and M. Alam, "Applications and trends of high performance computing for electric power systems: Focusing on smart grid," *IEEE Transactions on Smart Grid*, vol. 4, no. 2, pp. 922–931, 2013.

[3] A. Lanzon and I. R. Petersen, "Stability robustness of a feedback interconnection of systems with negative imaginary frequency response," *IEEE Transactions on Automatic Control*, vol. 53, no. 4, pp. 1042–1046, May 2008.

[4] N. Nikooienejad and S. O. Reza Moheimani, "Convex synthesis of SNI controllers based on frequency-domain data: MEMS nanopositioner example," *IEEE Transactions on Control Systems Technology*, vol. 30, no. 2, pp. 767–778, March 2022.

[5] C. Li, J. Wang, J. Shan, A. Lanzon, and I. R. Petersen, "Robust cooperative control of networked train platoons: A negative-imaginary systems' perspective," *IEEE Transactions on Control of Network Systems*, vol. 8, no. 4, pp. 1743–1753, Dec 2021.

[6] J. Wang, A. Lanzon, and I. R. Petersen, "Robust output feedback consensus for networked negative-imaginary systems," *IEEE Transactions on Automatic Control*, vol. 60, no. 9, pp. 2547–2552, Sep 2015.

[7] Y. Su, P. Bhowmick, and A. Lanzon, "A negative imaginary theory-based time-varying group formation tracking scheme for multi-robot systems: Applications to quadcopters," in *Proceedings of the 2023 IEEE International Conference on Robotics and Automation*, May-June 2023, pp. 1435–1441.

[8] ——, "Cooperative control of multi-agent negative imaginary systems with applications to UAVs, including hardware implementation results," in *Proceedings of the 2023 European Control Conference*, June 2023, pp. 1–6.

[9] A. Lanzon and H.-J. Chen, "Feedback stability of negative imaginary systems," *IEEE Transactions on Automatic Control*, vol. 62, no. 11, pp. 5620–5633, Nov 2017.

[10] M. A. Mabrok, A. G. Kallapur, I. R. Petersen, and A. Lanzon, "Generalizing negative imaginary systems theory to include free body dynamics: Control of highly resonant structures with free body motion," *IEEE Transactions on Automatic Control*, vol. 59, no. 10, pp. 2692–2707, Oct 2014.

[11] P. Bhowmick and A. Lanzon, "Output strictly negative imaginary systems and its connections to dissipativity theory," in *Proceedings of 58th IEEE Conference on Decision and Control*, Dec 2019, pp. 6754–6759.

[12] ——, "Time-domain output negative imaginary systems and its connection to dynamic dissipativity," in *Proceedings of 59th IEEE Conference on Decision and Control*, Dec 2020, pp. 5167–5172.

[13] ——, "Dynamic dissipative characterisation of time-domain input-output negative imaginary systems," *accepted in Automatica*, pp. 1–18, Oct 2023.

[14] P. Bhowmick, N. Bordoloi, and A. Lanzon, "Frequency-domain dissipativity analysis for output negative imaginary systems allowing imaginary-axis poles," in *Proceedings of the 2023 European Control Conference*, June 2023, pp. 1–6.

[15] A. Lanzon and P. Bhowmick, "Characterisation of input-output negative imaginary systems in a dissipative framework," *IEEE Transactions on Automatic Control*, vol. 68, no. 2, pp. 959–974, Feb 2023.

[16] J. Hu, B. Lennox, and F. Arvin, "Robust formation control for networked robotic systems using negative imaginary dynamics," *Automatica*, vol. 140, no. 110235, pp. 1–9, June 2022.

[17] P. Bhowmick, A. Ganguly, and S. Sen, "A new consensus-based formation tracking scheme for a class of robotic systems using negative imaginary property," *IFAC-PapersOnLine*, vol. 55, no. 1, pp. 685–690, 2022.

[18] J. J. Belletrutti and A. G. J. MacFarlane, "Characteristic loci techniques in multivariable-control-system design," *Proceedings of the Institution of Electrical Engineers*, vol. 118, no. 9, pp. 1291–1297, Sep 1971.

[19] A. G. J. Macfarlane and J. J. Belletrutti, "The characteristic locus design method," *Automatica*, vol. 9, no. 5, pp. 575–588, 1973.

[20] A. Bidram, A. Davoudi, F. L. Lewis, and J. M. Guerrero, "Distributed cooperative secondary control of microgrids using feedback linearization," *IEEE Transactions on Power Systems*, vol. 28, no. 3, pp. 3462–3470, 2013.

[21] A. Bidram, A. Davoudi, F. L. Lewis, and Z. Qu, "Secondary control of microgrids based on distributed cooperative control of multi-agent systems," *IET Generation, Transmission & Distribution*, vol. 7, no. 8, pp. 822–831, 2013.

[22] N. M. Dehkordi, N. Sadati, and M. Hamzeh, "Fully distributed cooperative secondary frequency and voltage control of islanded microgrids," *IEEE Transactions on Energy Conversion*, vol. 32, no. 2, pp. 675–685, 2017.

[23] A. Ganguly, S. Bhadra, P. Bhowmick, and S. Sen, "Distributed secondary control of islanded ac microgrids considering topology switching and plug-and-play operation," *IFAC-PapersOnLine*, vol. 55, no. 1, pp. 442–447, Feb 2022.